Received: 7 January 2026 | Revised: 19 June 2026 | Accepted: 21 June 2026

https://doi.org/10.1016/j.jtha.2026.06.033

ORIGINAL ARTICLE

The natural mutation Arg221aTrp in human α-thrombin abrogates physiological Na^+ binding and preferentially hinders the protease anticoagulant functions

Laura Acquasaliente[1] | Andrea Pierangelini[1] | Federico Uliana[2] | Anna Pagotto[1] | Alberto Covallero[1] | Daniele Peterle[1] | Serena Toffanin[3] | Cristiana Bulato[3] | Elena Campello[3] | Antonella Ciancetta[4] | Paolo Simioni[3] | Vincenzo De Filippis[1]

[1]Laboratory of Protein Chemistry, Department of Pharmaceutical and Pharmacological Sciences, University of Padua, Padua, Italy

[2]Department of Biology, Institute of Biochemistry, ETH Zürich, Zürich, Switzerland

[3]First Chair of Internal Medicine and Thrombotic and Haemorrhagic Diseases Unit, Department of Medicine, University Hospital of Padua, Padua, Italy

[4]Department of Chemical, Pharmaceutical and Agricultural Sciences, University of Ferrara, Ferrara, Italy

Correspondence
Vincenzo De Filippis, Department of Pharmaceutical and Pharmacological Sciences, School of Medicine, University of Padua, via Marzolo 5, Padua 35131, Italy.
Email: vincenzo.defilippis@unipd.it

Paolo Simioni, First Chair of Internal Medicine and Thrombotic and Haemorrhagic Diseases Unit, Department of Medicine, University Hospital of Padua, via Giustiniani, 2, 35128 Padua, Italy.
Email: paolo.simioni@unipd.it

Present addresses
Andrea Pierangelini, Nuffield Department of Medicine, Oxford University, Oxford, UK.

Federico Uliana, Johannes Gutenberg University of Mainz, 55128, Mainz, Germany.

Abstract

Background: Natural mutations in the prothrombin gene, involving the substitution of Arg596 with polar/apolar amino acids, represent an important risk factor for thrombosis. Notably, Arg596 in prothrombin corresponds to position 221a in the Na^+-binding loop of mature α-thrombin (αT). Patients carrying these mutations (Arg221a→Gln/Leu/Trp) share a common clinical phenotype, characterized by a moderately reduced procoagulant function in coagulation tests and resistance of αT variants to inactivation by antithrombin III (ATIII). However, the biochemical mechanisms linking these mutations to the increased thrombotic risk remain elusive.

Objectives: To provide quantitative data on the effect that the recombinant Arg221aTrp αT mutant (αT-PD2) has on the activation of procoagulant and anticoagulant pathways and elucidate the structural basis of the observed functional changes.

Methods: A multipronged approach was used, integrating recombinant DNA techniques, clotting/fibrinolytic and enzymatic assays, microscopy, proteomics, spectroscopic, mass spectrometry, and molecular modeling techniques.

Results: Arg221aTrp mutation abrogates physiological Na^+ binding and reduces the proportion of the fully active αT conformation. αT-PD2 affects procoagulant pathways by less efficiently generating fibrin (7-fold) and activating platelets (10-fold). The mutation potently affects anticoagulant pathways, as αT-PD2 is less efficiently inhibited by ATIII (3-fold), binds heparin less tightly (10-fold), and much less efficiently (41-fold) activates protein C.

Conclusion: Our data indicate that the procoagulant phenotype, observed in Arg221aTrp mutation carriers, may result from opposing inhibitory effects on both

Manuscript handled by: Ton Lisman

Final decision: Ton Lisman, 21 June 2026

© 2026 The Author(s). Published by Elsevier Inc. on behalf of International Society on Thrombosis and Haemostasis. This is an open access article under the CC BY license (http://creativecommons.org/licenses/by/4.0/).

Anna Pagotto, Department of Biology, Institute of Molecular Systems Biology, ETH Zürich, Zürich, Switzerland.

Daniele Peterle, Peptone Experimental Research Facility, Bellinzona, Switzerland.

Funding information
This work was supported by a grant from the Cassa di Risparmio di Padova e Rovigo Foundation Excellence Research Project (Bacterial Proteases in Thrombosis and Amyloidosis n. 52012) to V.D.F. and a grant from the Italian Ministry of University and Research (MIUR) (PRIN-2022 n. 2022ZSA2JP) to P.S.

procoagulant and anticoagulant pathways, with the impact on anticoagulant pathways being predominant and shifting the natural anticoagulant↔procoagulant equilibrium *in vivo* toward thrombosis.

KEYWORDS
antithrombin, genetic mutations, natural thrombin variants, thrombophilia, venous thromboembolism

1 | INTRODUCTION

Prothrombin (ProT) is the physiological zymogen precursor of α-thrombin (αT), the final effector serine protease of the coagulation cascade [1]. αT is generated in the prothrombinase complex on the surface of activated platelets after cleavage by factor [F]Xa at Arg271↓Thr272, to form the intermediate zymogen prethrombin 2 (Pre2), and at Arg320↓Ile321, to yield the mature active protease [2]. According to the Huber–Bode mechanism of zymogens activation [3], the NH_3^+-group of the N-terminal Ile16 (chymotrypsin numbering), generated after proteolytic activation of ProT, makes a high-energy salt bridge with Asp524 (Asp194, chymotrypsin numbering) and drives opening/ordering of the active site and surrounding regions in the catalytically competent conformation [4].

αT displays both procoagulant and anticoagulant functions in hemostasis [5]. The procoagulant function mainly involves the conversion of soluble fibrinogen (Fb) into insoluble fibrin and proteolytic activation of type-1 protease-activated receptor (PAR1) on platelets, which become bioadhesive. The anticoagulant function of αT entails proteolytic activation of protein C (PC), which inactivates the procoagulant cofactors V and VIII. Beyond the active site, most of αT interactions are mediated by 2 positively charged patches, ie, exosite-I and -II. Exosite-I is responsible for the binding of Fb, PAR1, and thrombomodulin (TM), a cofactor in PC activation by αT, whereas exosite II binds heparin, platelet glycoprotein-Ibα, and the elongated γ′-chain splice variant of Fb [1,6,7]. A key modulator of αT function is sodium ion (Na^+) [8], which binds to a specific site (shaped by the 180- and 220-loop) [9,10] and allosterically drives a conformational transition from a more closed and dynamic structure (the Na^+-free "slow" form) of the enzyme to a more open and rigid conformation (the Na^+-bound "fast" form) [11–13]. The 2 forms activate the anticoagulant PC with a comparable efficiency in the presence of Ca^{+2} and TM, whereas the Na^+-bound form more efficiently cleaves the procoagulant substrates Fb and PAR1 [14].

Almost 3 decades ago, the gain-of-function mutation c.*97G>A(G20210A) was identified in the ProT *F2* gene [15], resulting in moderate increase of thrombotic risk. More recently, heterozygous missense mutations in the *F2* gene (c.1787G>T, c.1787G>A, c.1786C>T) were found to be associated with moderate to severe hereditary thrombophilia [16–19]. These mutations result in the substitution of the positively charged Arg596 in the *F2* gene expression product with neutral and less polar amino acids, such as Leu (p.Arg596Leu:prothrombin Yukuhashi) [16], Gln (p.Arg596Gln:-prothrombin Belgrade and Amrita) [18,19], and Trp (p.Arg596Trp:-prothrombin Padua-2) [17]. The mutation of Arg596 represents an important risk factor for thrombosis [17,20,21], comparable with inherited deficiencies of natural anticoagulant factors PC or protein S [22], and indeed >60% of heterozygous carriers of Arg596-mutations develop venous thromboembolism (VTE) during their life [20]. Patients with Arg596 mutation share a common clinical phenotype, often referred to as AntiThrombin Resistance phenotype [23], which is generally characterized by (1) normal levels of circulating ProT variants in FII:Ag determinations, (2) only moderately (if any) reduced procoagulant function in clinical coagulation tests (prothrombin time and activated partial thromboplastin time), and (3) resistance of the mature αT variants to inactivation by ATIII [16–18]. These assays report in a cumulative fashion on the final effect of the mutation on hemostasis [16–19]. However, they can hardly contribute to unveil the mechanism(s) linking the change in the primary structure of αT to the increased thrombotic risk observed in patients with mutated Arg596.

To fill this gap of knowledge, here we expressed, purified to homogeneity, and thoroughly characterized the recombinant mutant of mature active αT (αT-PD2) in which Arg221a (chymotrypsinogen numbering) was replaced by Trp. Using a wide array of techniques, here we have comparatively studied the conformational and functional properties of wild-type (αT) and mutant αT-PD2 toward both procoagulant (Fb and PAR1) and anticoagulant substrates (PC) and inhibitors (ATIII). Biochemical data were interpreted on the modeled structure of αT-PD2 and indicate that the procoagulant phenotype, observed in Arg221aTrp mutation carriers, may result from the loss of Na^+-binding capacity in αT-PD2 and from a generalized decrease in the catalytic activity of the variant protease on both procoagulant and anticoagulant substrates, with the impact on anticoagulant pathways being predominant.

2 | MATERIALS AND METHODS

2.1 | Reagents

Ecarin from *Echis carinatus*, p-aminobenzamidine (PABA), (D)-Phe-Pro-Arg-chloromethyl ketone (PPACK), unfractionated heparin, salts, solvents, and reagents were purchased from Merck-Life-Science. Human PC and active protease (aPC), plasmin, ATIII, and rabbit TM were from Prolytix. Human plasma Fb was from American Diagnostica, while chromogenic substrates were purchased from Chromogenix. (D)-Phe-Pip-Arg-OH (FPR), Hir(1–47), hirugen, PAR1(38–60), and hirudin were produced as described [24–28].

2.2 | Methods

An extended/detailed version of the Methods is included in the Supplementary Materials.

Mutagenesis of the synthetic human prethrombin-2 (Pre2) cDNA, cloning expression, purification, and chemical characterization of mature wild-type αT and αT-PD2 mutant was carried out as described [26,29,30]. Whole blood (WB) samples were taken from 3 healthy donors, citrate treated, recalcified, and used in all analyses. Platelet-poor plasma samples were prepared as detailed [31,32]. WB samples were taken from a heterozygous patient with VTE, carrying the mutation at Arg596 in the *F2* gene expression product, which has been already enrolled in our previous study [17]. Donors gave their written informed consent to participate in this study, which was approved by the Institutional Ethics Committee of the Padua University Hospital.

Fibrin generation and degradation assays were carried out by turbidimetric measurements [31,33] (Table 1, Supplementary Figure S2). Fibrin structure was investigated by laser scanning confocal microscopy (LSCM) using a solution of AlexaFluor488-human Fb-conjugate (Thermo Fisher) and naïve Fb in Hepes Buffered Saline (HBS), and a Zeiss-LSM800 microscope (Carl Zeiss). Platelet aggregation assays were performed in WB using a Multiple Electrode Aggregometer (MEA) from Dynabyte [31,33]. Thrombin generation (TG) assays in WB were performed on a Fluoroskan-Ascent microplate fluorometer (Thermo LabSystems, Helsinki, Finland) [34].

The kinetic constants of S2238 and PAR1(38-60) hydrolysis were determined as described [33]. Thrombin-mediated PC activation was carried out in both a continuous and a discontinuous assay using the substrate S2366 [26], while thrombin inhibition by ATIII was performed as described [35].

The workflow of high-throughput protease screen (HTPS) is detailed elsewhere [32,36,37]. Peptide fragments were analyzed by liquid chromatography tandem mass spectrometry, using an Orbitrap Q-Exactive^{+} mass spectrometer (Thermo Fisher) coupled to an EASY-nLC-1000 liquid chromatography system (Thermo Fisher).

Active thrombin concentration was determined by UV absorption on a Jasco model V-630 spectrophotometer [38] and by active-site titration [39]. Far-UV circular dichroism (CD) spectra were

TABLE 1 Kinetic parameters of the generation and degradation of fibrin produced by αT-PD2 and αT.

	αT-PD2				αT			
Fibrin generation[a]								
Experimental conditions	**t_c (min)**	**S_m ($\Delta A_u \cdot min^{-1}$)**	**t_m (min)**	**ΔA_{max} (AU)**	**t_c (min)**	**S_m ($\Delta A_u \cdot min^{-1}$)**	**t_m (min)**	**ΔA_{max}(AU)**
Purified Fb	10.3 ± 0.3	0.72 ± 0.02	17.1 ± 0.2	0.70 ± 0.01	0.9 ± 0.1	10.4 ± 0.3	1.4 ± 0.2	0.36 ± 0.01
Plasma	1.0 ± 0.1	0.11 ± 0.01	2.5 ± 0.1	0.83 ± 0.02	0.15 ± 0.01	0.17 ± 0.01	0.3 ± 0.1	0.18 ± 0.01
Fibrin degradation[b]								
Experimental conditions	**LT (min)**	**TLT (h)**	**CLT (h)**	**V ($\Delta A_u \cdot min^{-1}$)**	**LT (min)**	**TLT (h)**	**CLT (h)**	**V ($\Delta A_u \cdot min^{-1}$)**
Purified Fb	23 ± 1	20 ± 2	11 ± 1	0.081 ± 0.002	131 ± 5	23 ± 2	14 ± 1	0.042 ± 0.005

Clotting parameters: t_c is the time of the lag phase, from the addition of thrombin until the apparent Abs of the solution increases by 0.01 AU and is calculated from the intercept of the straight-line tangent to the flex point of the clotting curve with the *x*-axis; S_m is the maximal rate of polymerization and is calculated from the slope of the straight-line tangent to the flex point of the clotting curve; t_m is the time needed to reach S_m from the addition of thrombin; ΔA_{max} is the maximal change of apparent Abs measured at the plateau phase. Fibrinolysis parameters: LT is the lysis time, ie, the time from the addition of plasmin to the preformed fibrin clot until the apparent Abs of the solution decreases by 0.01 AU; TLT is the total lysis time, corresponding to the time needed for complete clot dissolution, and can be determined as the time from adding plasmin until the time point when the apparent Abs almost reaches the baseline; CLT is the clot lysis time, which was defined as the time from the midpoint of the clear to maximum turbid transition, which characterizes clot formation, to the midpoint of the maximum turbid to clear transition, which represents clot lysis; V is the average rate of fibrin lysis and can be calculated from the slope of the descending limb of the curve between the time point of plasmin addition and the end point of TLT. A graphical illustration of clotting and fibrinolysis parameters is shown in Figure S2.

[a] Parameters extracted from the clotting curves in Figure 1A and B.

[b] Parameters extracted from the fibrinolysis curves in Figure 1B.

recorded on a Jasco J-810 spectropolarimeter, while fluorescence spectra were recorded on a Jasco FP-6500 spectropolarimeter [40]. Urea-induced denaturation experiments were performed as described [11,39].

PABA binding was monitored by fluorescence spectroscopy, as described [33]. For the binding of FPR, Hir(1-47), hirugen, and heparin, the emission of thrombin at the λ_{max} was measured as a function of ligand concentration [39,41]. For Na^+ binding, measurements were performed at 0.7M ionic strength. Surface plasmon resonance (SPR) was performed on a Biacore X-100 instrument from GE-Healthcare in HEPES Buffered Saline with EDTA and Surfactant P20 [31]. Rabbit TM was covalently immobilized via amine coupling reaction on a CM5 sensor chip and challenged with increasing concentrations of thrombin in the mobile phase.

Hydrogen/deuterium exchange mass spectrometry (HDX-MS) experiments were performed using an Automation-2.0 workstation (Waters), coupled to an Acquity UPLC M-class and a high-resolution Q-TOF-Xevo-G2S mass spectrometer (Waters). Plots of deuterium incorporation were generated using the DynamX 3.0 software (Waters) [32,41–43].

The 3-dimensional model of αT-PD2 was obtained using the crystallographic structure of the thrombin mutant Ile16Thr (PBD ID:6PXJ) [44] as a template. The QuickPrep, Loop-Modeler, and Protein-Builder modules, as implemented in the Molecular Operating Environment (MOE) suite, ver. 2024.06 (The Chemical Computing Group ULC), were used to model αT-PD2 structure. Electrostatic potential calculations were carried out using the APBS-Adaptive Poisson-Boltzmann Solver ver.3.0 [45] and the PDBQR software [46], using Chemistry at Harvard Macromolecular Mechanics parameters for protein residues and the Na^+ ion. For comparative analyses, the structure of thrombin in the Na^+-bound form was considered (1SG8.pdb) [10]. Images were generated using PyMOL Open Source ver.2.5.0.

Unless otherwise specified, all measurements are reported as the average of 3 independent experiments with SD as the error bars. Wilcoxon-test applications were used and the results were considered significant (*) when $P < .05$.

3 | RESULTS

3.1 | Production and chemical characterization of recombinant αT-PD2

Arg596 in the *F2* gene expression product corresponds to Arg553 in the circulating ProT zymogen and to Arg221a in the mature active αT (chymotrypsinogen numbering). Hereafter, we used the mature αT numbering (Arg221aTrp). Recombinant wild-type (αT) and Arg221aTrp mutant (αT-PD2) were produced with high purity (>95%), as previously detailed [31], and their chemical identity established by peptide mass fingerprint analysis (Supplementary Figure S1, Supplementary Table S1).

3.2 | αT-PD2 less efficiently generates fibrin from human plasma or isolated Fb

Turbidimetric analyses (Figure 1A, Supplementary Figure S2, Table 1) indicate that αT-PD2 generates fibrin from human plasma and isolated Fb much less efficiently than αT. In particular, the clotting time (t_c) measured with αT-PD2 is prolonged by ~7- and 11-fold in the plasma or isolated Fb solution, compared with αT, whereas the maximal change of apparent absorbance (ΔA_{max}) is increased by 4- and 2-fold in the plasma or purified Fb solution, suggesting that αT-PD2 more slowly generates fibrin, which contains thicker fibers than those produced with αT [47].

The parameters extracted from the clotting curves are consistent with the slower kinetics of substrate hydrolysis by αT-PD2 and with altered fibrin structure. The efficiency (k_{cat}/K_m) with which αT-PD2 releases fibrinopeptides A (FpA) and B (FpB) from purified Fb is 25- or 7.5-fold lower than that of αT, respectively (Figure 1C, Table 2), whereas the variant hydrolyzes S2238 (a thrombin-specific substrate) only 2-fold less efficiently (Figure 1D, Table 2). Furthermore, direct visualization of the 2 clots by LSCM (Figure 1E) indicates that αT-PD2 induces the formation of a less dense fibrin network, composed of fewer and thicker fibers, whereas in the presence of αT a clot formed by many and thinner fibers is obtained.

The different structure of fibrin network generated by αT or αT-PD2 is also reflected in the different kinetics of fibrinolysis of the 2 clots (Figure 1B, Table 1). Indeed, fibrin generated after 8-hour incubation of purified Fb with T-PD2 is degraded by plasmin more efficiently and with a shorter lag phase (Supplementary Figure S2) than that formed by αT under identical experimental conditions. Our results are consistent with earlier work showing that the number of fibers per volume, rather than individual fiber diameter, determines the resistance of fibrin to plasmin [48].

3.3 | αT-PD2 less efficiently triggers PAR1-mediated activation of platelets

The ability of αT-PD2 to agglutinate platelets in WB was tested by MEA [31,49] showing that αT-PD2 activates platelets much less efficiently than αT (Figure 2A), with a normalized area under the curve (AUC) value ~11-fold lower than that estimated for αT (Figure 2B). Likewise, αT-PD2 cleaves PAR1(38–60), ie, a synthetic peptide substrate reproducing the extracellular domain of PAR1 on platelets [26,27], with an efficiency 16-fold lower than that of αT (Figure 2C, Table 2).

3.4 | Arg221aTrp mutation impairs αT-mediated PC activation in a TM-independent manner

The efficiency with which αT-PD2 converts PC into the aPC was determined in both a continuous and a discontinuous assay

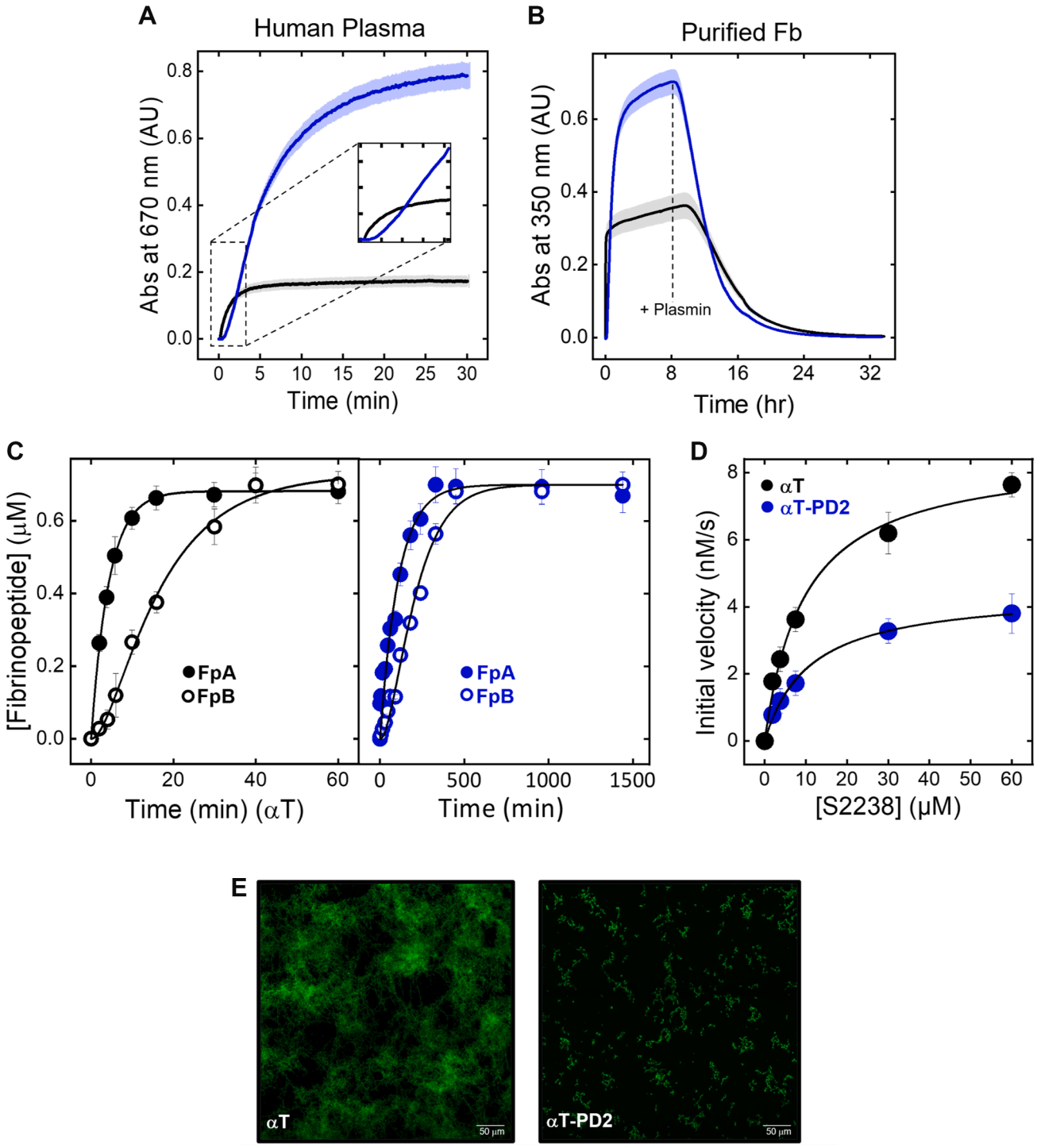


FIGURE 1 Fibrin generation and degradation by αT and αT-PD2 in human plasma and purified fibrinogen (Fb) solution. (A, B) Turbidimetric analysis of fibrin generation induced by αT (▬) and αT-PD2 (╍) on diluted (1:2) human plasma with HBS (A) or purified Fb solutions in HBS (B). The kinetics of fibrin generation, after protease addition (1 nM), was followed at 37 ± 0.1 °C by recording the apparent absorbance change at 670 or 350 nm, as indicated. (Panel A, Inset) Close-up view of the clotting curves in the 0-4-minute time range. (B) Turbidimetric analysis of fibrin degradation kinetics. After 8 hours of fibrin generation from purified Fb solutions, plasmin (50 nM) was added to the fibrin gels and the time course decrease of turbidity was recorded at 350 nm. From each curve, characteristic clotting (t_c, S_m, t_m, and A_{max}) and lysis (LT, TLT, CLT, and V) parameters were extracted and reported in Table 1 (Supplementary Figure S2). (C) Kinetics of FpA (filled circles) and FpB (empty circles) release from purified Fb solution (0.35 μM) in the presence of αT (●, ○) or αT-PD2 (●, ○). Reactions were carried out at 37± 0.1 °C in HBS and quantified by RP-HPLC. The data points were interpolated with eqs. 1 and 2 (Supplementary Materials) to yield the values of k_{cat}, K_m, and k_{cat}/K_m of FpA and FpB release (Table 2). (D) Kinetic analysis of S2238 hydrolysis by αT (●) or αT-PD2 (●). The initial rate of pNA release from S2238 was determined at 37 ± 0.1 °C by recording the absorbance of HBS solutions at 405 nm as a function of [S2238] in the presence of 50 pM αT or αT-PD2. The data points were interpolated with eq. 3 (Supplementary Materials) to yield the kinetic parameters reported in Table 2. (E) Representative laser scanning confocal microscopy images of fibrin clots obtained after a 5-hour

(Figure 3A, B and Table 2), using the chromogenic substrate S2366 (pGlu-Pro-Arg-pNA) for aPC [29]. In continuous assays, control experiments indicate that the substrate is only poorly cleaved by αT or αT-PD2 (Figure 3A). Our data indicate that, in the presence of TM, αT-PD2 activates PC much less efficiently than αT by 89-fold (continuous assay) or 41-fold (discontinuous assay). Notably, in the absence of TM, PC activation by αT-PD2 was only barely (if at all) detectable. The relative differences in PC activation, observed between wild-type and variant protease in the 2 assays, can be ascribed to the fact that in the continuous assay the additional cleavage of S2366 by thrombin is not considered.

SPR measurements indicate that the affinity of thrombin for immobilized TM is not substantially reduced by the mutation (Figure 3C, Supplementary Figure S3, Table 3). These results provide evidence that the drop in PC activation by αT-PD2 is predominantly caused by a decrease in the efficiency with which the variant cleaves PC zymogen rather than to a decrease in the affinity for TM.

3.5 | Arg221aTrp mutation reduces αT inhibition by ATIII

The potency with which ATIII inhibits αT-PD2 or αT in the absence of heparin was determined in a discontinuous assay [35], allowing to estimate for αT-PD2 a pseudo-first-order association rate constant (k_a) of thrombin-inhibitor complex 2.7-fold lower than that measured with αT (Figure 3D, Table 2). When ATIII inhibition was studied in the presence of heparin, inhibition assays were carried out continuously to yield the value of the second-order association rate constant (k_1) at each heparin [H] concentration [35] (Figure 3E). From the plot of k_1 values as a function of [H] (Figure 3F), it was possible to determine the optimal heparin concentration, $[H]_{opt}$, at which k_1 value is maximal, k_1°. As expected, in the presence of heparin, the value of k_1° is strongly increased for both wild-type and variant thrombin. Even in the presence of heparin, αT-PD2 is inhibited by ATIII 2.8-fold less efficiently than αT (Table 2). Noteworthy, the heparin concentration that is required for optimal inhibition of αT-PD2 by ATIII is increased by 4-fold compared with αT.

3.6 | TG in WB

TG assays were performed in the absence and presence of TM [34]. The following thrombogram parameters were considered: (1) lag-time (the time it takes for the clotting reaction to begin), (2) peak thrombin (the maximum concentration of active thrombin generated during the blood clotting process), and (3) endogenous thrombin potential (ETP, the total amount of thrombin generated). The results in Supplementary Figure S4 indicate a reduced responsiveness to TM in the proband, compared with healthy controls. Addition of TM had a pronounced effect on TG in the controls, with ETP and peak thrombin values reduced by 49% and 43% of their baseline values, respectively. In contrast, the proband exhibited only a moderate reduction of these parameters, with ETP and peak thrombin values decreasing by only 32% or 22% of the baseline levels. These data are compatible with a functional impairment of the PC pathway [34].

3.7 | Proteomic analysis of αT-PD2 substrate specificity

The HTPS proteomic method [36] was exploited to investigate the substrate specificity of αT-PD2 on the proteome wide scale (Supplementary Figure S5A). HTPS analysis demonstrates that recombinant αT-PD2 has reduced proteolytic activity compared with that of recombinant or natural αT. After 2-hour digestion, indeed, the number of identified cleavages for αT-PD2 (5.390) was only 35% or 38% as that determined for recombinant (15.291 unique cleavages) or natural (13.862 unique cleavages) αT (Supplementary Figure S5B, S5E). Nevertheless, HTPS analysis shows that αT-PD2 essentially retains the substrate specificity profile of wild-type/natural αT, with a well-known preference for Arg and Lys at position P1 and Pro at P2 [36]. However, a statistically significant broader specificity is observed with αT-PD2 at positions P3, P4, and P4′ (Supplementary Figure S5C, S5D).

3.8 | Conformational characterization of αT-PD2

3.8.1 | Spectroscopic analysis of αT-PD2

The far-UV CD spectrum of αT-PD2 differs from that of αT in both shape and intensity (Supplementary Figure S6A). Although these changes may argue for an altered secondary structure content of αT-PD2, a merely spectroscopic (nonconformational) contribution of Trp221a to the spectrum of the protease variant should also be adequately considered [11].

Fluorescence spectra indicate that, despite the presence of a further Trp-residue in αT-PD2 (10 Trp-residues instead of 9), the emission of αT-PD2 is approximately half as that of αT (Supplementary Figure S6B), suggesting that on average Trp-residues in the variant are in a more flexible chemical environment [50]. Furthermore, stability measurements indicate that αT-PD2

incubation of naïve Fb (2.5 mg/ml), containing 10% (w/w) of AlexaFluor488-labeled Fb solution, with 0.9 nM αT (*left panel*) or αT-PD2 (*right panel*) in HBS at 25 ± 0.1 °C. The scale size is indicated by white bars. Unless othewise specified, the data points results from the average of 3 independent measurements (n = 3), with error bars as ±SD. The shaded area in panels A and B represents the standard deviation of the turbidimetric signal at each time point. CLT, clot lysis time; HBS, HEPES buffered saline; LT, lysis time; RP-HPLC, reversed phase high performance liquid chromatography; TLT, total lysis time; V, average rate of fibrin lysis.

TABLE 2 Enzyme kinetic parameters of substrate hydrolysis by αT-PD2 and αT.

	αT-PD2			αT			
Substrate/inhibitor	k_{cat}/K_m ($\mu M^{-1}\cdot sec^{-1}$)	k_{cat} (sec^{-1})	K_m (μM)	k_{cat}/K_m ($\mu M^{-1}\cdot sec^{-1}$)	k_{cat} (sec^{-1})	K_m (μM)	r^k (αT/αT-PD2)
S2238[a]	8 ± 1	89 ± 2	11 ± 1	17 ± 3	171 ± 8	10 ± 1	2.1
FpA[b]	0.51 ± 0.05			12.5 ± 0.6			25.0
FpB[b]	0.49 ± 0.04			3.7 ± 0.8			7.5
PAR1 (38-60)[c]	2.7 ± 0.6			43.3 ± 1.5			16.0
	k_{cat}/K_m ($mM^{-1}\cdot sec^{-1}$)			k_{cat}/K_m ($mM^{-1}\cdot sec^{-1}$)			
PC + TM[d] (continuous)	1.63 ± 0.02			145.5 ± 0.7			89.0
PC + TM[j] (discontinuous)	4.95 ± 0.78			203 ± 17			41.0
	k_a[g] ($M^{-1}\cdot sec^{-1}$)			k_a[g] ($M^{-1}\cdot sec^{-1}$)			
AT-III[e,g]	0.45 ± 0.02 × 10^4			1.22 ± 0.03 × 10^4			2.7
	$k_1°$[h] ($M^{-1}\cdot sec^{-1}$)	$[H]_{opt}$[i] (nM)		$k_1°$[h] ($M^{-1}\cdot sec^{-1}$)	$[H]_{opt}$[i] (nM)		
AT-III + H[f]	1.46 ± 0.01 × 10^6	155		4.09 ± 0.02 × 10^6	38		2.8

[a] Data extracted from Figure 1D.
[b] Data extracted from Figure 1C.
[c] Data extracted from Figure 2C.
[d] Continuous assay: data extracted from Figure 3A.
[e] Data extracted from Figure 3D.
[f] Data extracted from Figure 3E.
[g] k_a is the pseudo-first-order association kinetic rate constant of ATIII binding to thrombin.
[h] $k_1°$ is the maximal value of the second-order association rate constant of ATIII binding to thrombin (k_1).
[i] $[H]_{opt}$ is the concentration of heparin at which k_1 is maximal ($k_1°$).
[j] Discontinuous assay: data extracted from Figure 3B.
[k] r is the ratio between the specificity constants of thrombin-mediated substrate hydrolysis (ie, k_{cat}/K_m) or between the kinetic constants of ATIII association to thrombin (k_a, $k_1°$).

($[urea]_{1/2}$ = 2.0 ± 0.1M) is substantially less stable to urea denaturation than αT ($[urea]_{1/2}$ = 2.7 ± 0.1 M) (Supplementary Figure S6C).

3.8.2 | Probing the structure of αT-PD2 by site-specific ligand binding

The conformation of hot spots in αT-PD2 and αT was probed using the site-specific perturbation approach [33,39]. Affinity measurements were carried out by measuring fluorescence changes at 25 °C in Tris buffered saline, pH 7.4, containing 150 mM NaCl (Table 3, Supplementary Figure S7).

The structure of αT-PD2 active site was probed using competitive inhibitors of incremental size, ie, PABA [51], FPR [24], and Hir(1-47) [4,52–54]. In particular, PABA binds to Asp189 in the protease primary S1 site, while FPR and Hir(1-47) variably interact with S1-S2-S3 sites. Hir(1-47) covers the S1 site, binds to the S2 and S3 sites, and also makes contacts with the γ-loop and Na^+-binding site. The conformational state of exosite-I and II in αT-PD2 was probed with hirugen [55] or heparin [56]. Our data show that, contrary to what was observed with αT, binding of FPR, Hir(1-47), and Na^+ to αT-PD2 causes a decrease of fluorescence intensity (Supplementary Figure S7B, C, F), suggesting that the responsiveness of the thrombin fold to ligand binding is different in αT and αT-PD2.

Our data indicate that the substrate recognition sites in αT-PD2 are only moderately perturbed, because the affinity of the protease variant for the inhibitors is changed by only ±1.6- to 2.4-fold, compared with αT. The binding strength of hirugen to αT-PD2 is reduced by 2.5-fold, whereas the affinity of heparin is decreased by 10-fold, thus suggesting that exosite II (but not exosite-I) is substantially perturbed in αT-PD2. Importantly, our data report a 35-fold drop in the affinity of αT-PD2 for Na^+ at 25 °C, with a K_d value going from 21±3 mM (αT) to 737±61 mM (αT-PD2). These results suggest that Na^+-binding to the protease variant *in vivo* is severely compromised. Indeed, under physiological conditions of temperature (37 °C) and sodium concentration (145 mM), the Na^+-bound form of αT-PD2 would be only marginally populated (<4%), compared with αT (55%) [57]. The loss of Na^+ binding, inferred from spectroscopic data, is corroborated by enzyme kinetics experiments (Supplementary Figure S8). As expected, the rate of S2238 hydrolysis by αT substantially increases in a saturation manner with NaCl concentration (0.1-0.4 M), consistent with the well-known Na^+-dependent activation of αT [8]. At variance, the activity of αT-PD2 remains roughly constant and only slightly (if at all) increases at 0.4 M NaCl.

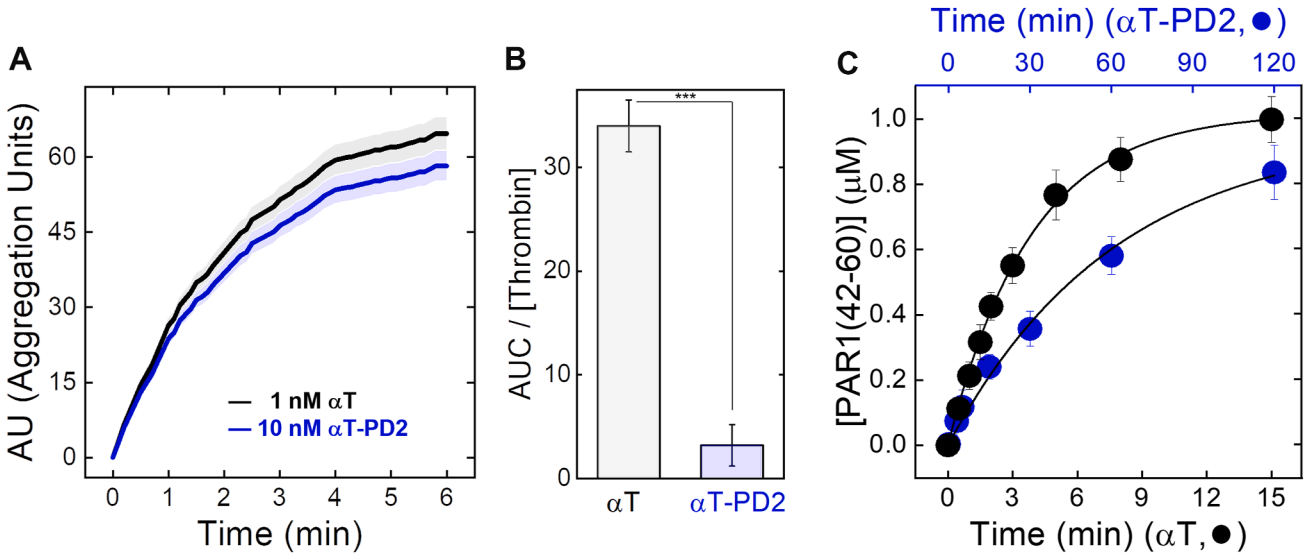


FIGURE 2 Effect of αT and αT-PD2 on platelet aggregation and PAR1 cleavage. (A) Impedance aggregometry analysis of platelet aggregation induced by αT or αT-PD2. Representative MEA curves were obtained at 37 ± 0.1°C after addition of αT (1.0 nM) or αT-PD2 (10 nM) to HBS diluted (1:2) whole blood (190,000 platelets/μl). (B) Histogram of the platelet aggregating effect of αT or αT-PD2, as obtained in panel A. For each measurement, the area under the curve (AUC) was normalized for the corresponding thrombin concentration. Each AUC value is the average of single determinations on blood samples from 3 healthy donors (n = 3), with error bars as ±SD. Significant differences were obtained by Wilcoxon test and are indicated by lines connecting the data being compared (***$P < .001$). (C) Time course analysis of 1 μM PAR1(38-60) cleavage by 100 pM αT (●) or αT-PD2 (●). The reaction was carried out at 25 °C in TBS and the time course of PAR1(42-60) fragment release quantified by RP-HPLC. The data points were fitted with eq. 4 (Supplementary Materials) describing the kinetics of product formation under enzyme:substrate pseudo-first-order condition, to yield the values of k_{cat}/K_m reported in Table 2. The data points are the average of 3 independent measurements (n = 3), with error bars as ±SD. TBS, Tris buffered saline.

Altogether, our results indicate that exosite II and especially the Na^+-binding site are strongly perturbed in αT-PD2, whereas the active site and exosite-I are only moderately altered.

3.8.3 | HDX-MS analysis of αT-PD2 structure

HDX-MS is a well-established technique in structural biology [58] and takes advantage of the intrinsic propensity of protein backbone amide hydrogens located at flexible/exposed sites to undergo H/D exchange at much higher rates than those which are embedded at more rigid/buried sites. HDX can be monitored by recording the time-dependent mass increase of short fragments, generated after proteolysis with pepsin, allowing to obtain a sequence-dependent profile, predominantly of protein dynamics, with a spatial resolution of 3 to 6 amino acids [32,41–43].

HDX experiments were conducted in parallel with αT-PD2 and αT under identical and carefully controlled experimental conditions, at 25 °C in sodium phosphate buffer, pD 7.2, containing 0.4M NaCl. Notably, at this temperature and NaCl concentration, αT is almost fully saturated (>95%) with Na^+, whereas αT-PD2 is predominantly (>70%) in the Na^+-free form. After proteolysis with pepsin, 79 and 78 fragments were identified in αT-PD2 or αT, yielding a sequence coverage >87% and a redundancy of 3.0 in both cases (Supplementary Figure S9). A bidimensional butterfly plot of deuterium uptake, reporting the time-dependent difference of deuterium incorporation between αT and αT-PD2, is reported in Figure 4A. To more clearly identify the regions that are conformationally altered in αT-PD2, ΔHDX values measured after a 2-hour-incubation with D_2O were projected onto on the crystallographic structure of natural thrombin (1ppb) [59] (Figure 4B).

Analysis of the ΔHDX profile (Figure 4A) shows a moderate and generalized increase of deuterium uptake in αT-PD2 that argues for a globally enhanced conformational flexibility of the variant protease, compared with αT. This result is consistent with the remarkably lower fluorescence intensity that has been measured for αT-PD2 (Supplementary Figure S6B). Furthermore, a remarkable increase in deuterium incorporation (ΔHDX > 0.8Da) was observed at specific sites in αT-PD2: (1) the N-terminal region (^{16}Ile-Glu^{23}) of the B-chain, in the activation site (see below), (2) the β-strand ^{130}Leu-Leu^{144}, linking α-helix ^{125}Asp-Leu^{129c} to the γ-loop, and (iii) the region ^{161}Pro-Phe^{181}, encompassing the helix ^{165}Arg-Thr^{172} and contributing to both the S3 specificity subsite (Thr172, Ile174, and Ile176) and exosite II (Arg165, Lys169). At variance, His^{57} and Ser^{195} (in the catalytic site) and Asp^{194} (in the activation site) are almost fully protected from H/D exchange, even at longer incubation times (2 hours) in both αT and αT-PD2. As reported above, the N-terminal region ^{16}Ile-Glu^{23} is significantly more dynamic/accessible in αT-PD2, compared with αT. This finding suggests that the NH_3^+-group of Ile16 in the variant protease structure is not stably bound to the carboxylate of Asp194 side chain, allowing the N-terminus to "swing" in and out the activation pocket and reduce the proportion of the protease

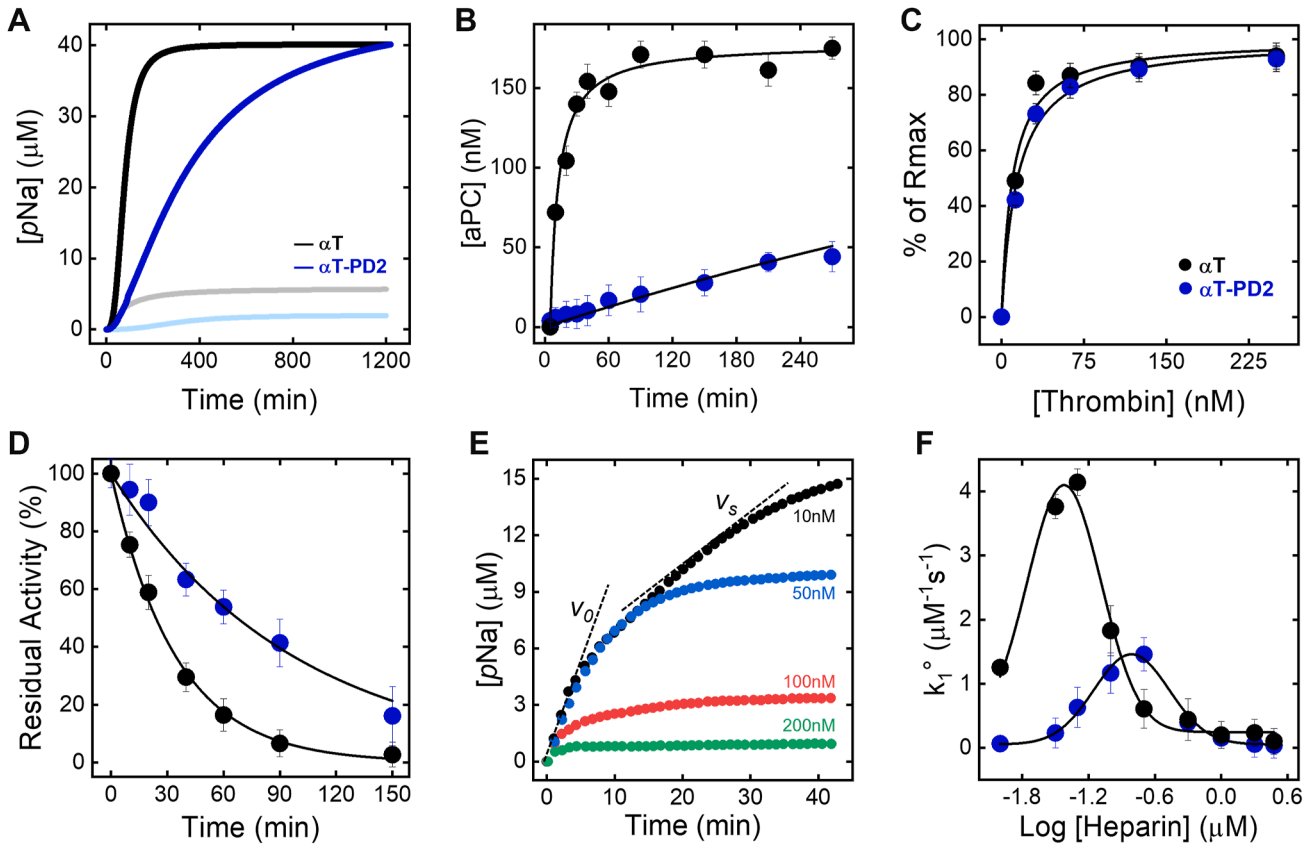


FIGURE 3 Effect of Arg221aTrp mutation on thrombin-mediated PC activation and thrombin inhibition by antithrombin III (ATIII). (A, B) PC activation. (A) Representative progress curves of aPC generation by αT-PD2 (▬) and αT (▬) in the continuous assay. The experimental conditions were 0.1 nM thrombin, 50 nM TM, 10 nM PC, and 45 μM S2366 in HBS, pH 7.4, 5 mM $CaCl_2$, 0.1% PEG-8000 at 37 ± 0.1 °C. Control experiments in the absence of PC were carried out with 0.1 nM αT (▬) and αT-PD2 (▬). The sigmoidal nature of the progress curves, most visible in the case of the less active αT-PD2, is the result of the continuous nature of the assay that measures S2366 hydrolysis after the buildup of aPC. (B) In the discontinuous assay, PC (230 nM) was incubated with thrombin (4 nM) and TM (50 nM). At time points, aliquots were taken and diluted (30-fold) with a solution containing 200 μM S2366 and 1 μM hirudin, to block thrombin activity. The release of pNA from S2366 was monitored at 405 nm. The data points were interpolated with eq. 4 to extract the k_{cat}/K_m values of PC activation by thrombin (Table 2). In the discontinuous assay, no lag phase is observed because activation of PC is determined by quenching the thrombin-catalyzed reaction at different times under pseudo-first-order kinetics. (C) SPR analysis of αT-PD2 (●) and αT (●) binding to immobilized TM (Supplementary Figure S3). Measurements were performed at 25°C and analyzed in the affinity mode, to extract the K_d values (Table 2). (D) Discontinuous assay of αT (●) and αT-PD2 (●) inhibition by ATIII (40 nM). At time points, the residual protease activity was determined by measuring the release of pNA from S-2238 (20 μM). The data points were interpolated with eqs. 5 and 6 (Supplementary Materials) to yield the pseudo-first-order association kinetic constant, k_a (Table 2). (E) Continuous assay of αT (●) and αT-PD2 (●) inhibition by ATIII (40 nM) in the presence of heparin (10 nM to 3 μM). The curve describing the release of pNA as a function of time was fitted to eq. 7 (Supplementary Materials) to extract the values of v_0, v_s, and k_{obs}. From these parameters, the second-order association rate constant (k_1) could be calculated. (F) Plot of k_1 values as a function of [heparin]. The data points for αT (●) and αT-PD2 (●) were interpolated with eq. 9 (Supplementary Materials) to estimate the optimal heparin concentration, $[H]_{opt}$, at which k_1 value is maximal, $k_1°$ (Table 2). Unless otherwise specified, measurements were carried out in HBS, pH 7.4, 0.1% PEG-8000 at 37 ± 1 °C, and the data points are the average of 3 independent measurements (n = 3), with error bars as ±SD.

existing in the fully active form, ie, with the salt bridge Ile16-Asp194 properly formed.

3.9 | Molecular modeling and electrostatic properties αT-PD2

αT-PD2 structure was modeled on the crystallographic coordinates of a thrombin mutant in which isoleucine (Ile)16 in the activation domain was replaced by threonine (Thr) (6PXJ) [44]. Noteworthy, the structure of Ile16Thr mutant was chosen as a template, as it recapitulates (at least qualitatively) the key functional properties highlighted above for αT-PD2. Therefore, it is expected that even the 3-dimensional structure of αT-PD2 might resemble that of Ile16Thr. The mutant, in fact, binds sodium 70-fold less tightly than the wild-type enzyme, activates the anticoagulant PC 30-fold less efficiently, and is much less active toward Fb and PAR1.

TABLE 3 Affinity of site-specific ligands for αT-PD2 and αT.

Ligand	K_d[a] αT-PD2	K_d[a] αT	r[b]	ΔΔG$_b$ (kcal/mole)[c]
PABA	368 ± 66 μM	151 ± 10 μM	2.4	+ 0.53
FPR	31.1 ± 3.7 μM	15.3 ± 3.2 μM	2.0	+ 0.42
Hir(1-47)	61 ± 5 nM	99 ± 16 nM	0.6	- 0.29
Hirugen	2.8 ± 0.4 μM	1.1 ± 0.3 μM	2.5	+ 0.55
Heparin	60.2 ± 10.1 μM	6.3 ± 0.6 μM	9.6	+ 1.34
Na^+	737 ± 61 mM	21 ± 3 mM	35.1	+ 2.11
TM	15 ± 2 nM	10 ± 2 nM	1.5	+ 0.24

[a] The values of the equilibrium dissociation constants (K_d) of the ligand–thrombin complexes were extracted from the data reported in Figure S7.
[b] $r = K_d$ (αT-PD2)/K_d (αT).
[c] $\Delta\Delta G_b = \Delta G_b$ (αT-PD2) − ΔG_b (αT) = $RT \cdot \ln[K_d(\alpha T\text{-PD2})/K_d(\alpha T)]$ is the difference free energy change of binding between the variant and wild-type thrombin, where R is the gas constant and T the absolute temperature.

The 3-dimensional model αT-PD2 was obtained by keeping the position of all atoms in the template structure unchanged and substituting *in silico* Arg221a with Trp, and Thr16 back to Ile (Supplementary Materials). The structure of αT in the Na^+-bound form was used for comparison (1SG8.pdb) [10]. Structure superposition (Figure 5A–F) suggests that the 190-loop, containing Asp189 in the S1 site and the uncompensated Glu192 at the entrance of the active-site cleft, is significantly displaced toward the active site, which becomes less accessible. The 180- and 220-loop, shaping the Na^+-binding site, are largely disorganized in αT-PD2, consistent with the drop in the affinity for Na^+. The γ-loop and the 170-helix become more flexible, as a result of disruption of the salt bridges (ie, Glu146-Arg221a and Glu164-Lys185) linking these regions to the Na^+-binding site in αT. Furthermore, the hydrogen-bond network stabilizing the oxyanion hole is altered in the variant protease. Finally, the salt bridge Ile16-Asp194 in the activation domain is substantially perturbed in αT-PD2, consistent with our HDX-MS data (Figure 4).

Thrombin has a highly asymmetric distribution of positive and negative amino acids [4,39] (Figure 5H). The active-site pocket is negatively charged and surrounded by a "negative ring" of uncompensated acidic residues, mainly located in the protease insertion loops and opposed by 2 electropositive patches, exosite-I and -II. Figure 5G shows a significant rearrangement of the surface electrostatic potential in αT-PD2. In particular, the active site becomes more electronegative, along with the γ-loop, the Na^+-binding site, and the apolar S3 subsite, whereas exosites I and II become less electropositive. These changes likely reflect (1) the ablation of the electropositive Arg221a, (2) the release of the positive Na^+ ion, and (3) the concomitant disruption of the salt bridges stabilizing the Na^+-binding site, whereby several negatively charged amino acids are left electrostatically uncompensated (eg, Glu146 in the γ-loop and Glu164 in the 170-helix).

4 | DISCUSSION

Among inherited factors predisposing to VTE, loss-of-function mutations in anticoagulant protein genes (ATIII, PC, and protein S) and gain-of-function mutations in some procoagulant protein genes (FV, FVIII, and FIX) [60–62] induce clinically severe hypercoagulable conditions [22,63–66]. In the past, prothrombotic gain-of-function mutations (G20210A) have been identified also in the prothrombin *F2* gene [15] and, more recently, 3 additional prothrombotic mutations, all affecting position 596 (Arg→Leu/Gln/Trp), have been detected in the *F2* gene expression product of patients from Japan [16,23], Serbia [18], India [19], Italy [17], and China [21].

The *in vitro* results reported in this study indicate that the final thrombotic phenotype observed in patients with Arg596→Trp mutation might be the consequence of a loss-of-function effect involving both procoagulant and anticoagulant pathways (Figures 1–3 and Tables 1–3). Proteomic analysis, conducted by HTPS (Supplementary Figure S4), demonstrates that αT-PD2 displays a generalized lower proteolytic activity which, however, variably impacts on the cleavage efficiency of physiological procoagulant (Fb and PAR1) and anticoagulant (PC and ATIII) pathways, with a resulting final procoagulant effect. In particular, αT-PD2 displays reduced procoagulant function, as it less efficiently releases FpA (25-fold) and FpB (7.5-fold) than αT and markedly prolongs the clotting time of Fb solutions (11-fold) or plasma samples (6.6-fold). αT-PD2 also plays a profibrinolytic effect by generating fibrin clots containing fewer and thicker fibers, which are degraded by plasmin much more efficiently than those produced by wild-type αT. The drop in the efficiency with which αT-PD2 cleaves PAR1 (25-fold) and activates platelets (11-fold) represents a further impairment of αT-PD2 procoagulant functions.

Arg221aTrp mutation also remarkably (and even more strongly) hinders the crucial anticoagulant pathways of αT, entailing inhibition by ATIII and activation of PC. In fact, after a 60-minute incubation with ATIII, the residual activity of αT-PD2 was >54%, whereas that of αT was only 16%. Furthermore, αT-PD2 binds heparin 10-fold less tightly than αT and the optimal concentration of heparin necessary to achieve maximal ATIII inhibition is 4-fold higher with αT-PD2. Reduction in the affinity for heparin argues for a looser interaction of αT-PD2 with negatively charged anticoagulant glycosaminoglycans (eg, heparan sulfates), which line the microvasculature and facilitate αT-ATIII encounter *in vivo*, with a resulting indirect procoagulant effect. More importantly, αT-PD2 activates PC zymogen at least 41-fold less efficiently than αT in the presence of TM and this effect appears to be caused by a reduced efficiency with which αT-PD2 activates PC rather than by a decrease in the affinity of TM for the variant protease. It is noteworthy that, without TM, αT-PD2 only negligibly (if at all) activates PC. It is important to note that the remarkable decrease in PC activation evoked by αT-PD2 *in vitro*, with soluble TM and thrombin, may not necessarily reflect the process occurring on the vascular endothelial cell surface, where thrombin is bound to TM, and PC is bound to the endothelial PC receptor [60]. Hence, we carried out TG assays in WB in the presence and absence of TM, using blood samples from healthy controls and from a VTE

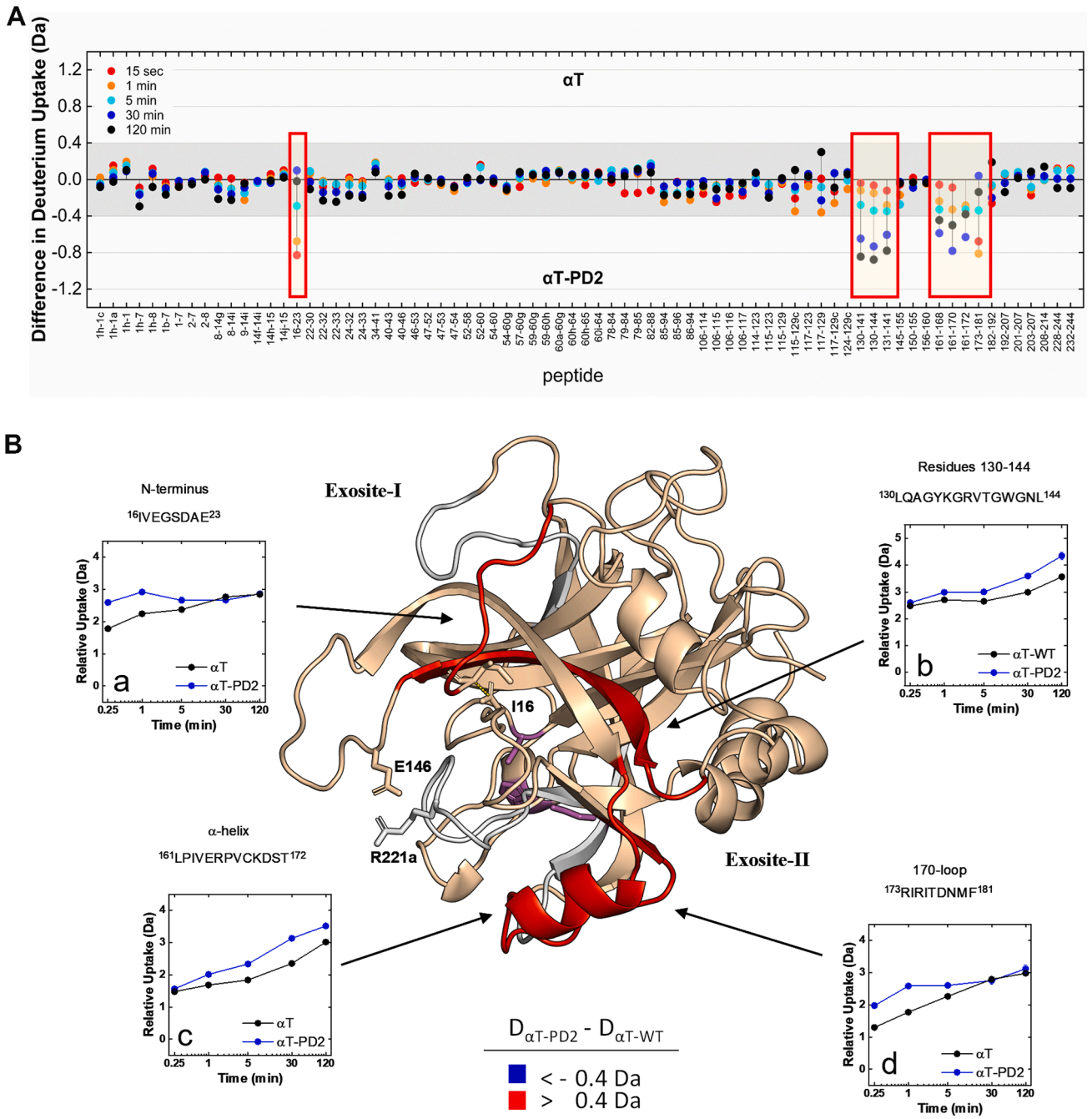
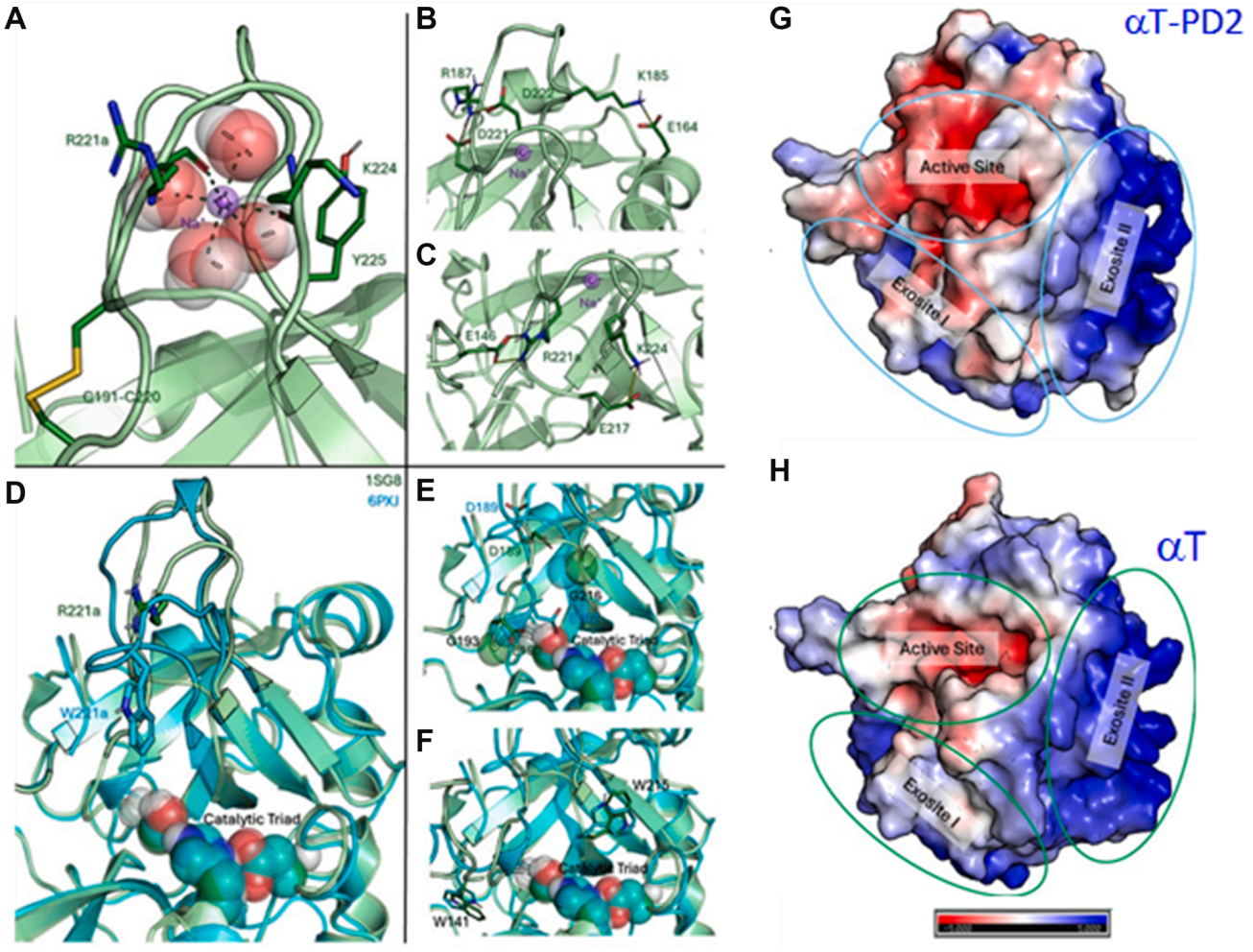


FIGURE 4 Bidimensional (A) and 3-dimensional (B) difference deuterium uptake plots of αT-PD2 relative to αT. (A) Changes in deuterium uptake, ΔHDX = HDX(αT) – HDX(αT-PD2), for each peptic fragment at increasing time points (15 seconds to 2 hours). For a given peptide, negative values of ΔHDX are indicative of a higher flexibility/exposure of that peptide in αT-PD2 structure relative to αT. Differences in deuterium uptake are considered significative if |ΔHDX| > 0.4Da. (B) Three-dimensional HDX difference map of deuterium uptake by αT-PD2 compared with αT after a 120-minutes H/D exchange time. The values of ΔHDX were mapped onto the crystal structure of αT (1ppb). Regions of αT-PD2 with |ΔHDX| > 0.4Da are colored red or blue according to their higher or lower deuterium uptake relative to αT. All other regions with |ΔHDX| < 0.4Da are colored light gold, while the regions that were not covered in the map (ie, ^{65}Leu-Glu^{77}, ^{95}Asn-Leu^{105}, and ^{215}Trp-Phe^{227}) are in light gray (Supplementary Figure S9). Catalytic amino acids (His57, Asp102, and Ser195) are shown in magenta. (Panels *a* to *d*) Kinetics of deuterium uptake of selected peptic fragments in αT-PD2 (●) and αT (●). Measurements were carried out with thrombin (1.25 μM) at 25 °C in 20 mM sodium phosphate, (95:5) D_2O:H_2O solution, pD 7.2, containing 0.4M NaCl. Data points are the average of 3 independent measurements, with errors as ±SD. Notably, SD was always < 0.1 and therefore in most cases masked by the symbols. HDX, hydrogen/deuterium exchange mass spectrometry.



I

Fb Aα	1	ADSGEG DFLAEGGGVR↓GPRVVE-RHQSACK -DSDWPFCSD	P02671
Fb Bβ	1	QGVNDNEEG FF-----SAR↓GHRPLDKKREEAPS LRPAPPPISG	P02675
PAR1	8	ATNA TL-----DPR↓SFLLR------NPN -DKYE-PFWE	P56488
PC	158	DTEDQED QV-----DPR↓LIDGK-------MT	P04070
ATIII	387	AV VI-----AGR↓SL---------NPN	P01008
Thrombin	exosite II	active site	S′groove exosite I	

FIGURE 5 Structural model and electrostatic properties of αT-PD2. (A) Close-up view of the Na^+-binding site in αT (1sg8.pdb). The sodium ion (violet sphere) is coordinated octahedrically by the carbonyl oxygens of Arg221a and Lys224 and by 4 water molecules. (B, C) The Na^+-site is stabilized by the salt bridges Asp221-Arg187-Asp222 and Glu217-Lys224, and by 2 additional salt bridges with the γ-loop (Arg221a-Glu146) and the 170-helix (Lys185-Glu164), at the perihery of exosite II. (D–F) Superposition of αT X-ray structure (green) and αT-PD2 model (cyan). In αT-PD2, the Na^+-site is disorganized and the stabilizing salt bridges broken; Asp189 side chain in the S1 site and Glu192 at the entrance of the catalytic cleft are displaced to reduce substrate accessibility; Trp141 and Trp215 side chains have different conformations in αT and αT-PD2. (G, H) Electrostatic potential (ζ) of αT-PD2 and αT, projected onto the solvent-excluded surface, colored according to the sign of ζ (blue, positive; red, negative), and expressed as kJ/(mol·q). The active site, the substrate recognition subsites, the γ-loop, and the Na^+-site are more electronegative in αT-PD2 than in αT, whereas exosites I and II become less electropositive. (I) Amino acid sequences of αT substrates/inhibitors. The sequences were aligned according to their 3-dimensional superposition in the complexes with αT, as deduced form crystallographic and modeling studies. Numbering refers to the sequence of the mature proteins. The UniProt code is reported on the right-handed column. The regions of thrombin in contact with the substrates are indicated. The arrows indicate the scissile bonds. Basic and acidic residues are colored blue and red, respectively. Images were generated using PyMOL Open Source ver. 2.5.0. and surfaces rendered with the Adaptive Poisson-Boltzmann Solver Electrostatics Plugin.

patient carrying the Arg596Trp heterozygous mutation in the *F2* gene expression product. Our results (Supplementary Figure S4) indicate a reduced responsiveness to TM in the proband, compared with healthy controls, compatible with a functional impairment of the PC pathway.

4.1 | Structural basis for the altered functional properties of αT-PD2

The model structure of αT-PD2 (Figure 5A–F) shows that the Na^+-binding site in αT-PD2 is strongly perturbed, consistent with the affinity loss of the variant protease for Na^+, as demonstrated experimentally in this study (Table 2). However, this is not surprising. Arginine, in fact, is highly polar, carries a net positive charge, and has a long and flexible side chain. At variance, tryptophan is the most hydrophobic and bulky among protein amino acids, and it has a rigid/planar side chain. The changes in the physicochemical properties of the amino acid at position 221a can alter local protein folding and force the protein backbone to assume a distorted conformation, not competent for Na^+ coordination.

Disordering of the Na^+-binding site leads to disruption of the salt bridges (ie, Arg221a-Glu146; Lys185-Glu164) linking the Na^+-site to the flanking regions encompassing the γ-loop and 170-helix. The importance of the integrity of the salt bridge Arg221a-Glu146 in promoting sodium binding is documented by the fact that the natural (pro)thrombin variants Frankfurt [61] and Salakta [62], both containing the mutation Glu146→Ala, show compromised Na^+ binding. Likewise, Arg221a→Ala mutation reduces by 5-fold the affinity of αT for Na^+ [10]. Perturbations in the Na^+-binding site and γ-loop are transmitted by spatial proximity to exosite-I and the active-site cleft, which becomes less accessible to substrates/inhibitors in αT-PD2. Furthermore, the crucial salt bridge Ile16-Asp194, stabilizing the active protease conformation, is also substantially perturbed in αT-PD2 (Figure 5), in keeping with experimental HDX-MS data (Figure 4). These changes are fully consistent with the decrease in the catalytic efficiency of αT-PD2, highlighted by enzymatic assays on specific procoagulant (Fb and PAR1) and anticoagulant (PC) substrates (Figures 1 and 2) and inhibitors (ATIII) (Figure 3), as well as by HTPS analysis of thrombin activity on a proteomic wide scale (Supplementary Figure S5).

Perturbation of the sodium-binding site and disruption of salt bridges within and outside the Na^+-site also impact on the electrostatics of αT-PD2 and the protease molecular recognition properties (Figure 5G, H). Electrostatic potential calculations show that the variant protease features a more negatively charged environment, compared with wild-type αT, in the active site and substrate recognition subsites, in the γ-loop, and the Na^+-binding site. Concomitantly, exosites I and II become less electropositive. These changes are expected to preferentially affect the affinity of those procoagulant (Fb and PAR1) [67–69] and anticoagulant (PC) [70,71] substrates and cofactors (heparin) [56,72] that primarily exploit favorable electrostatic coupling in order to be recognized (and cleaved) by thrombin (Figures S10 and S11). As shown in Figure 5I, these substrates display excess negative charge in the regions interacting with the protease active-site cleft and the exosites. The drop in the cleavage efficiency of these substrates, beyond structural perturbations in the active site of the variant protease, can be reasonably explained by the stronger electrostatic repulsion existing between the electronegative substrates and the more negative active-site region of αT-PD2 and, concomitantly, by the weaker electrostatic coupling of the negative substrates with the less electropositive exosites in the variant protease. In the case of ATIII, the 3-fold reduced inhibition of αT-PD2 is likely caused by perturbation of the binding surfaces in the variant protease. In fact, the reactive-center loop of ATIII makes extensive hydrophobic and polar/charge interactions with key residues in αT, ie, in the γ-loop, the Na^+-binding site (Lys224, Arg221a, and Glu217), and 170-helix [72]. Hence, perturbation of these regions can impair proper inhibitor–protease interaction.

5 | CONCLUSIONS

Our findings show that Arg221aTrp mutation in αT-PD2 impairs both procoagulant (fibrin generation and platelet activation) and anticoagulant (ATIII-mediated αT inhibition and PC activation) functions *in vitro*. However, the impact of the loss-of-function mutation on anticoagulant pathways is stronger and may shift the natural procoagulant↔anticoagulant equilibrium *in vivo* toward a hypercoagulable state and a final prothrombotic clinical phenotype.

AUTHOR CONTRIBUTIONS

L.A. and A. Covallero performed the biochemical work; A. Pierangelini, A. Pagotto, and D.P. performed HDX-MS work; F.U. performed HTPS analysis; S.T., C.B., and E.C. provided plasma samples and performed TG assays; A. Ciancetta carried out modeling work; P.S. inspired the work, designed research, and interpreted the data; L.A. and V.D.F. designed research and interpreted the data; V.D.F. coordinated the work and wrote the manuscript; all authors analyzed the data and reviewed the final version of the manuscript.

DATA AVAILABILITY

All reagents and data presented in this study are available from the corresponding author upon reasonable request.

DECLARATION OF COMPETING INTERESTS

There are no competing interests to disclose.

ORCID

Vincenzo De Filippis https://orcid.org/0000-0001-9775-8894

REFERENCES

[1] Di Cera E. Thrombin. *Mol Aspects Med*. 2008;29:203–54.

[2] Versteeg HH, Heemskerk JW, Levi M, Reitsma PH. New fundamentals in hemostasis. *Physiol Rev*. 2013;93:327–58.

[3] Huber R, Bode W. Structural basis of the activation and action of trypsin. *Acc Chem Res*. 1978;11:114–22.

[4] Bode W, Turk D, Karshikov A. The refined 1.9-A X-ray crystal structure of D-Phe-Pro-Arg chloromethylketone-inhibited human alpha-thrombin: structure analysis, overall structure, electrostatic properties, detailed active-site geometry, and structure–function relationships. *Protein Sci*. 1992;1:426–71.

[5] Di Cera E. Thrombin as procoagulant and anticoagulant. *J Thromb Haemost*. 2007;5:196–202.

[6] Huntington JA. Molecular recognition mechanisms of thrombin. *J Thromb Haemost*. 2005;3:1861–72.

[7] Bock PE, Panizzi P, Verhamme IM. Exosites in the substrate specificity of blood coagulation reactions. *J Thromb Haemost*. 2007;5:81–94.

[8] Wells CM, Di Cera E. Thrombin is a Na^+-activated enzyme. *Biochemistry*. 1992;31:11721–30.

[9] Di Cera E, Guinto ER, Vindigni A, Dang QD, Ayala YM, Wuyi M, Tulinsky A. The Na^+ binding site of thrombin. *J Biol Chem*. 1995;270:22089–92.

[10] Pineda AO, Carrell CJ, Bush LA, Prasad S, Caccia S, Chen ZW, Mathews FS, Di Cera E. Molecular dissection of Na^+ binding to thrombin. *J Biol Chem*. 2004;279:31842–53.

[11] De Filippis V, De Dea E, Lucatello F, Frasson R. Effect of Na^+ binding on the conformation, stability and molecular recognition properties of thrombin. *Biochem J*. 2005;390:485–92.

[12] Lechtenberg BC, Johnson DJ, Freund SM, Huntington JA. NMR resonance assignments of thrombin reveal the conformational and dynamic effects of ligation. *Proc Natl Acad Sci U S A*. 2010;107:14087–92.

[13] Ruben EA, Gandhi PS, Chen Z, Koester SK, DeKoster GT, Frieden C, Di Cera E. (19)F NMR reveals the conformational properties of free thrombin and its zymogen precursor prethrombin-2. *J Biol Chem*. 2020;295:8227–35.

[14] Dang OD, Vindigni A, Di Cera E. An allosteric switch controls the procoagulant and anticoagulant activities of thrombin. *Proc Natl Acad Sci U S A*. 1995;92:5977–81.

[15] Poort SR, Rosendaal FR, Reitsma PH, Bertina RM. A common genetic variation in the 3′-untranslated region of the prothrombin gene is associated with elevated plasma prothrombin levels and an increase in venous thrombosis. *Blood*. 1996;88:3698–703.

[16] Miyawaki Y, Suzuki A, Fujita J, Maki A, Okuyama E, Murata M, Takagi A, Murate T, Kunishima S, Sakai M, Okamoto K, Matsushita T, Naoe T, Saito H, Kojima T. Thrombosis from a prothrombin mutation conveying antithrombin resistance. *N Engl J Med*. 2012;366:2390–6.

[17] Bulato C, Radu CM, Campello E, Gavasso S, Spiezia L, Tormene D, Simioni P. New prothrombin mutation (Arg596Trp, Prothrombin Padua 2) associated with venous thromboembolism. *Arterioscler Thromb Vasc Biol*. 2016;36:1022–9.

[18] Djordjevic V, Kovac M, Miljic P, Murata M, Takagi A, Pruner I, Francuski D, Kojima T, Radojkovic D. A novel prothrombin mutation in two families with prominent thrombophilia—the first cases of antithrombin resistance in a Caucasian population. *J Thromb Haemost England*. 2013;11:1936–9.

[19] Sivasundar S, Oommen AT, Prakash O, Baskaran S, Biswas R, Nair S, Mohan CG, Biswas L. Molecular defect of 'Prothrombin Amrita': substitution of arginine by glutamine (Arg553 to Gln) near the Na(+) binding loop of prothrombin. *Blood Cells Mol Dis*. 2013;50:182–3.

[20] Miljic P, Gvozdenov M, Takagi Y, Takagi A, Pruner I, Dragojevic M, Tomic B, Bodrozic J, Kojima T, Radojkovic D, Djordjevic V. Clinical and biochemical characterization of the prothrombin Belgrade mutation in a large Serbian pedigree: new insights into the antithrombin resistance mechanism. *J Thromb Haemost*. 2017;15:670–7.

[21] Wu YF, Huang Y, Weng BH, Deng S, Pan LY, Li Z. Systemic thrombosis with prothrombin Belgrade mutation in a Chinese patient: a case report. *World J Clin Cases*. 2025;13:98390. https://doi.org/10.12998/wjcc.v13.i10.98390

[22] Rosendaal FR. Venous thrombosis: a multicausal disease. *Lancet*. 1999;353:1167–73.

[23] Kishimoto M, Suzuki N, Murata M, Ogawa M, Kanematsu T, Takagi A, Kiyoi H, Kojima T, Matsushita T. The first case of antithrombin-resistant prothrombin Belgrade mutation in Japanese. *Ann Hematol*. 2016;95:541–2.

[24] Krem MM, Di Cera E. Dissecting substrate recognition by thrombin using the inactive mutant S195A. *Biophys Chem*. 2003;100:315–23.

[25] De Filippis V, Quarzago D, Vindigni A, Di Cera E, Fontana A. Synthesis and characterization of more potent analogues of hirudin fragment 1-47 containing non-natural amino acids. *Biochemistry*. 1998;37:13507–15.

[26] Acquasaliente L, Peterle D, Tescari S, Pozzi N, Pengo V, De Filippis V. Molecular mapping of α-thrombin/β2-glycoprotein I (β2GpI) interaction reveals how beta2GpI affects alphaT functions. *Biochem J*. 2016;473:4629–50.

[27] Lancellotti S, Rutella S, De Filippis V, Pozzi N, Rocca B, De Cristofaro R. Fibrinogen-elongated gamma chain inhibits thrombin-induced platelet response, hindering the interaction with different receptors. *J Biol Chem*. 2008;283:30193–204.

[28] Vindigni A, De Filippis V, Zanotti G, Visco C, Orsini G, Fontana A. Probing the structure of hirudin from Hirudinaria manillensis by limited proteolysis. Isolation, characterization and thrombin-inhibitory properties of N-terminal fragments. *Eur J Biochem*. 1994;226:323–33.

[29] Pozzi N, Acquasaliente L, Frasson R, Cristiani A, Moro S, Banzato A, Pengo V, Scaglione GL, Arcovito A, De Cristofaro R, De Filippis V. β2-Glycoprotein I binds to thrombin and selectively inhibits the enzyme procoagulant functions. *J Thromb Haemost*. 2013;11:1093–102.

[30] Sokolov AV, Acquasaliente L, Kostevich VA, Frasson R, Zakharova ET, Pontarollo G, Vasilyev VB, De Filippis V. Thrombin inhibits the anti-myeloperoxidase and ferroxidase functions of ceruloplasmin: relevance in rheumatoid arthritis. *Free Radic Biol Med*. 2015;86:279–94.

[31] Acquasaliente L, Pontarollo G, Radu CM, Peterle D, Artusi I, Pagotto A, Uliana F, Negro A, Simioni P, De Filippis V. Exogenous human α-Synuclein acts in vitro as a mild platelet antiaggregant inhibiting α-thrombin-induced platelet activation. *Sci Rep*. 2022;12:9880.

[32] Pagotto A, Uliana F, Cavedon E, Nordio G, Pierangelini A, Acquasaliente L, Macchia ML, Bellanda M, Gatto B, De Silvestro G, Marson P, Gregori D, Simioni P, Picotti P, De Filippis V. The main protease (M^{pro}) from SARS-CoV-2 triggers plasma clotting in vitro by activating coagulation factors VII and FXII. *Commun Biol*. 2025;8:1145.

[33] Pontarollo G, Acquasaliente L, Peterle D, Frasson R, Artusi I, De Filippis V. Non-canonical proteolytic activation of human prothrombin by subtilisin from *Bacillus subtilis* may shift the procoagulant–anticoagulant equilibrium toward thrombosis. *J Biol Chem*. 2017;292:15161–79.

[34] Zanetto A, Campello E, Bulato C, Willems R, Konings J, Roest M, Gavasso S, Nuozzi G, Toffanin S, Burra P, Russo FP, Senzolo M, de Laat B, Simioni P. Impaired whole blood thrombin generation is associated with procedure-related bleeding in acutely decompensated cirrhosis. *J Hepatol*. 2025;82:1023–35.

[35] Arcone R, Chinali A, Pozzi N, Parafati M, Maset F, Pietropaolo C, De Filippis V. Conformational and biochemical characterization of a

biologically active rat recombinant Protease Nexin-1 expressed in *E. coli*. *Biochim Biophys Acta*. 2009;1794:602–14.

[36] Uliana F, Vizovišek M, Acquasaliente L, Ciuffa R, Fossati A, Frommelt F, Goetze S, Wollscheid B, Gstaiger M, De Filippis V, Auf dem Keller U, Aebersold R. Mapping specificity, cleavage entropy, allosteric changes and substrates of blood proteases in a high-throughput screen. *Nat Commun*. 2021;12:1693.

[37] Wiśniewski JR. Filter-aided sample preparation for proteome analysis. *Methods Mol Biol*. 2018;1841:3–10.

[38] Fontana A, Zambonin M, De Filippis V, Bosco M, Polverino de Laureto P. Limited proteolysis of cytochrome c in trifluoroethanol. *FEBS Lett*. 1995;362:266–70.

[39] Pozzi N, Zerbetto M, Acquasaliente L, Tescari S, Frezzato D, Polimeno A, Gohara DW, Di Cera E, De Filippis V. Loop electrostatics asymmetry modulates the preexisting conformational equilibrium in thrombin. *Biochemistry*. 2016;55:3984–94.

[40] De Filippis V, Vassiliev VB, Beltramini M, Fontana A, Salvato B, Gaitskhoki VS. Evidence for the molten globule state of human apoceruloplasmin. *Biochim Biophys Acta*. 1996;1297:119–23.

[41] Acquasaliente L, Pierangelini A, Pagotto A, Pozzi N, De Filippis V. From haemadin to haemanorm: synthesis and characterization of full-length haemadin from the leech *Haemadipsa sylvestris* and of a novel bivalent, highly potent thrombin inhibitor (haemanorm). *Protein Sci*. 2023;32:e4825. https://doi.org/10.1002/pro.4825

[42] Peterle D, Pontarollo G, Spada S, Brun P, Palazzi L, Sokolov AV, Spolaore B, Polverino de Laureto P, Vasilyev VB, Castagliuolo I, De Filippis V. A serine protease secreted from *Bacillus subtilis* cleaves human plasma transthyretin to generate an amyloidogenic fragment. *Commun Biol*. 2020;3:764.

[43] De Filippis V, Acquasaliente L, Pierangelini A, Marin O. Chemical synthesis and structure–activity relationship studies of the coagulation factor Xa inhibitor tick anticoagulant peptide from the hematophagous parasite ornithodoros moubata. *Biomimetics (Basel)*. 2024;9:485.

[44] Stojanovski BM, Chen Z, Koester SK, Pelc LA, Di Cera E. Role of the I16-D194 ionic interaction in the trypsin fold. *Sci Rep*. 2019;9:18035. https://doi.org/10.1038/s41598-019-54564-6

[45] Konecny R, Baker NA, McCammon JA. iAPBS: a programming interface to Adaptive Poisson–Boltzmann Solver (APBS). *Comput Sci Discov*. 2012;5:015005. https://doi.org/10.1088/1749-4699/5/1/015005

[46] Dolinsky TJ, Nielsen JE, McCammon JA, Baker NA. PDB2PQR: an automated pipeline for the setup of Poisson–Boltzmann electrostatics calculations. *Nucleic Acids Res*. 2004;32:W665–7.

[47] Weisel JW, Nagaswami C. Computer modeling of fibrin polymerization kinetics correlated with electron microscope and turbidity observations: clot structure and assembly are kinetically controlled. *Biophys J*. 1992;63:111–28.

[48] Wolberg AS. Thrombin generation and fibrin clot structure. *Blood Rev*. 2007;21:131–42.

[49] Tóth O, Calatzis A, Penz S, Losonczy H, Siess W. Multiple electrode aggregometry: a new device to measure platelet aggregation in whole blood. *Thromb Haemost*. 2006;96:781–8.

[50] Chen Y, Barkley MD. Toward understanding tryptophan fluorescence in proteins. *Biochemistry*. 1998;37:9976–82.

[51] Evans SA, Olson ST, Shore JD. p-Aminobenzamidine as a fluorescent probe for the active site of serine proteases. *J Biol Chem*. 1982;257:3014–7.

[52] De Filippis V, Colombo G, Russo I, Spadari B, Fontana A. Probing the hirudin–thrombin interaction by incorporation of noncoded amino acids and molecular dynamics simulation. *Biochemistry*. 2002;41:13556–69.

[53] De Filippis V, Russo I, Vindigni A, Di Cera E, Salmaso S, Fontana A. Incorporation of noncoded amino acids into the N-terminal domain 1-47 of hirudin yields a highly potent and selective thrombin inhibitor. *Protein Sci*. 1999;8:2213–7.

[54] De Filippis V, Acquasaliente L, Pontarollo G, Peterle D. Noncoded amino acids in protein engineering: structure–activity relationship studies of hirudin–thrombin interaction. *Biotechnol Appl Biochem*. 2018;65:69–80.

[55] Vijayalakshmi J, Padmanabhan KP, Mann KG, Tulinsky A. The isomorphous structures of prethrombin2, hirugen-, and PPACK-thrombin: changes accompanying activation and exosite binding to thrombin. *Protein Sci*. 1994;3:2254–71.

[56] Carter WJ, Cama E, Huntington JA. Crystal structure of thrombin bound to heparin. *J Biol Chem*. 2005;280:2745–9.

[57] Griffon N, Di Stasio E. Thermodynamics of Na^+ binding to coagulation serine proteases. *Biophys Chem*. 2001;90:89–96.

[58] Masson GR, Burke JE, Ahn NG, Anand GS, Borchers C, Brier S, Bou-Assaf GM, Engen JR, Englander SW, Faber J, Garlish R, Griffin PR, Gross ML, Guttman M, Hamuro Y, Heck AJR, Houde D, Iacob RE, Jørgensen TJD, Kaltashov IA, et al. Recommendations for performing, interpreting and reporting hydrogen deuterium exchange mass spectrometry (HDX-MS) experiments. *Nat Methods*. 2019;16:595–602.

[59] Rydel TJ, Tulinsky A, Bode W, Huber R. Refined structure of the hirudin–thrombin complex. *J Mol Biol*. 1991;221:583–601.

[60] Dahlbäck B, Villoutreix BO. Regulation of blood coagulation by the protein C anticoagulant pathway: novel insights into structure–function relationships and molecular recognition. *Arterioscler Thromb Vasc Biol*. 2005;25:1311–20.

[61] Degen SJ, McDowell SA, Sparks LM, Scharrer I. Prothrombin Frankfurt: a dysfunctional prothrombin characterized by substitution of Glu-466 by Ala. *Thromb Haemost*. 1995;73:203–9.

[62] Miyata T, Aruga R, Umeyama H, Bezeaud A, Guillin MC, Iwanaga S. Prothrombin Salakta: substitution of glutamic acid-466 by alanine reduces the fibrinogen clotting activity and the esterase activity. *Biochemistry*. 1992;31:7457–62.

[63] Simioni P, Cagnin S, Sartorello F, Sales G, Pagani L, Bulato C, Gavasso S, Nuzzo F, Chemello F, Radu CM, Tormene D, Spiezia L, Hackeng TM, Campello E, Castoldi E. Partial F8 gene duplication (factor VIII Padua) associated with high factor VIII levels and familial thrombophilia. *Blood*. 2021;137:2383–93.

[64] Wischmeyer JT, Baird CH, Grandvallet Contreras J, Tran A, Phang T, Liu T, Manco-Johnson MJ. A naturally occurring gain-of-function mutation in factor VIII. *N Engl J Med*. 2025;393:722–4.

[65] Simioni P, Tormene D, Tognin G, Gavasso S, Bulato C, Iacobelli NP, Finn JD, Spiezia L, Radu C, Arruda VR. X-linked thrombophilia with a mutant factor IX (factor IX Padua). *N Engl J Med*. 2009;361:1671–5.

[66] Crous-Bou M, Harrington LB, Kabrhel C. Environmental and genetic risk factors associated with venous thromboembolism. *Semin Thromb Hemost*. 2016;42:808–20.

[67] Stubbs MT, Oschkinat H, Mayr I, Huber R, Angliker H, Stone SR, Bode W. The interaction of thrombin with fibrinogen. A structural basis for its specificity. *Eur J Biochem*. 1992;206:187–95.

[68] Rose T, Di Cera E. Substrate recognition drives the evolution of serine proteases. *J Biol Chem*. 2002;277:19243–6.

[69] Gandhi PS, Chen Z, Di Cera E. Crystal structure of thrombin bound to the uncleaved extracellular fragment of PAR1. *J Biol Chem*. 2010;285:15393–8.

[70] Fuentes-Prior P, Iwanaga Y, Huber R, Pagila R, Rumennik G, Seto M, Morser J, Light DR, Bode W. Structural basis for the anticoagulant activity of the thrombin–thrombomodulin complex. *Nature*. 2000;404:518–25.

[71] Pozzi N, Barranco-Medina S, Chen Z, Di Cera E. Exposure of R169 controls protein C activation and autoactivation. *Blood*. 2012;120:664–70.

[72] Li W, Johnson DJ, Esmon CT, Huntington JA. Structure of the antithrombin–thrombin–heparin ternary complex reveals the antithrombotic mechanism of heparin. *Nat Struct Mol Biol*. 2004;11:857–62.

SUPPLEMENTARY MATERIALS

The following supporting information can be downloaded at https://doi.org/10.1016/j.jtha.2026.06.033. Extended methods. Supplementary Table S1: Mass values and identification of the tryptic fragments derived from Pre2-PD2. Supplementary Figure S1: Purity check and chemical characterization of recombinant Pre2-PD2 and αT-PD2. Supplementary Figure S2: Turbidimetric curve of fibrin generation and degradation. Supplementary Figure S3: SPR analysis of thrombin binding to immobilized TM. Supplementary Figure S4: TG in WB. Supplementary Figure S5: Characterization of αT-PD2 substrate specificity by HTPS analysis. Supplementary Figure S6: Spectroscopic characterization of αT-PD2 conformation and stability. Supplementary Figure S7: Binding of site-specific ligands to αT and αT-PD2. Supplementary Figure S8: Effect of NaCl on the rate of substrate hydrolysis by wild-type and variant thrombin. Supplementary Figure S9: Sequence coverage of αT-PD2 after peptide mass fingerprint analysis. Supplementary Figure S10: Three-dimensional structure of thrombin bound to the procoagulant substrates. Supplementary Figure S11: Three-dimensional structure of thrombin bound to anticoagulant substrates and cofactors.